Cement & Concrete Composites 33 (2011) 702–715

Contents lists available at ScienceDirect

Cement & Concrete Composites

journal homepage: www.elsevier.com/locate/cemconcomp

Relationships between microstructural properties and compressive strength of consolidated and unconsolidated cemented paste backfills

Erol Yilmaz [a,b,c], Tikou Belem [a,b,c,*], Bruno Bussière [a,b], Mostafa Benzaazoua [a,b,c,d]

[a] Université du Québec en Abitibi-Témiscamingue (UQAT), Department of Applied Sciences, 445 Boul. de l'Université, Rouyn-Noranda, Québec, Canada J9X 5E4
[b] Industrial NSERC-Polytechnique-UQAT Chair on Environment and Mine Waste Management, Canada
[c] Canada Research Chair on Integrated Management of Sulphidic Mine Tailings Using Backfill Technology, Canada
[d] Laboratoire de Génie Civil et d'Ingénierie Environnementale, INSA de Lyon, Bât. Sadi Carnot, 9, rue de la physique, 69621 Villeurbanne cedex, France

ARTICLE INFO

Article history:
Received 19 October 2009
Received in revised form 29 March 2011
Accepted 30 March 2011
Available online 12 April 2011

Keywords:
Paste backfill
CUAPS
Mercury porosimetry
Pore structure
Compressive strength
Curing conditions

ABSTRACT

Few studies have been so far done on the pore structure behaviour of cemented paste backfill (CPB) samples cured under pressure, which might be more representative of the field conditions. This is most likely due to a lack of suitable laboratory equipment and test procedures. In this paper, the effects of curing conditions on changes in CPB microstructure and corresponding unconfined compressive strength (UCS) were assessed using both an improved laboratory apparatus called CUAPS (curing under applied pressure system) and conventional plastic moulds. The CUAPS-consolidated and plastic mould-unconsolidated CPB samples were prepared with a slag-based binder which is a blend of 20 wt.% of ordinary Portland cement and 80 wt.% of blast furnace slag. CPB microstructural properties are compared for binder contents of 3, 4.5 and 7 wt.%, and curing times of 7, 14 and 28 days. Mercury intrusion porosimetry (MIP) results show that changes in intrusion porosity (and thus in microstructure) strongly depend on the water-to-cement (*w/c*) ratio and drainage conditions (consolidated *vs.* unconsolidated). Indeed, as *w/c* ratio decreases or curing time increases, total porosity is reduced, mainly due to the reduction in larger-sized pores by partial filling with cementitious phases. Specific surface area (SSA) measurements show good correlation with UCS values, meaning that the UCS of unconsolidated CPB increases with increasing SSA. Different regression models between UCS and MIP parameters (threshold diameter, total-, meso-, and macro-porosity) and SSA of CPB are also proposed and discussed.

1. Introduction

Cemented paste backfill (CPB) is increasingly used in the mining industry due to technical, economical and environmental benefits. CPB provides secondary ground support for cost-effective mining operations and greater safety for mine workers, generates lower capital and operating costs than rockfills and hydraulic fills, and reduces surface tailings disposal by diverting them into underground openings or stopes, thereby reducing environmental hazards and tailings management costs [1–4]. Given all these practical benefits, CPB is usually more cost effective and versatile than other backfill types.

CPB is a cementitious material produced with three ingredients: (1) filtered mine tailings (containing typically 70–85 wt.% solid), (2) hydraulic binders (1–7 wt.% by dry mass of tailings), and (3) mixing water to ensure the paste's flowability in the pipeline for final deposition [5]. The composition of CPB determines its long-term strength and durability. Many researchers have examined the effects of different parameters (e.g., tailings granularity, binder type, and content) on the short- and long-term strength and stability of CPB over different curing times [6–18]. The service life and durability of CPB structure also depend on its material properties, in situ placement, and curing conditions, as well as its self-weight consolidation. A number of researchers [17,19–29] shown experimentally that curing CPB under pressure increases its unconfined compressive strength (UCS) development due to pore water pressure dissipation and solid skeleton settlement. Moreover, some of these studies showed that, in addition to UCS, other properties such as saturated hydraulic conductivity, specific surface area (SSA), porosity, and diffusivity change significantly during curing due to microstructure changes in hardened materials [14,30–32].

A number of recent studies have evaluated the microstructural properties of CPB materials by mercury intrusion porosimetry (MIP) testing [13,15,21,31,33–40,71]. Results show that CPB pore structure is greatly affected by the tailings grain size distribution (GSD), water-to-cement (*w/c*) ratio, mixing water quality, curing conditions (e.g., under applied pressure), binder type, and mix

* Corresponding author at: Université du Québec en Abitibi-Témiscamingue (UQAT), Department of Applied Sciences, 445 Boul. de l'Université, Rouyn-Noranda, Québec, Canada J9X 5E4. Tel.: +1 819 762 0971x2359; fax: +1 819 797 4727.
E-mail address: Tikou.Belem@uqat.ca (T. Belem).

0958-9465/$ - see front matter Crown Copyright © 2011 Published by Elsevier Ltd. All rights reserved.
doi:10.1016/j.cemconcomp.2011.03.013

proportions over curing times. Ouellet [15] showed that total porosity of CPB samples, indicated by mercury intrusion in conventional plastic moulds, remained almost the constant during curing. Little information is available on the effects of curing under pressure on CPB pore structure behaviour. To our knowledge, no microstructural investigation based on MIP has been conducted so far on CPB samples cured under pressure, which might be more representative of the field conditions. This is most likely due to a lack of suitable laboratory equipment and test procedures. Consequently, aspects related to CPB in situ curing conditions that can significantly affect its pore structure need further investigation. To develop adequate experimental setups and suitable procedures for preparing laboratory samples of mine backfill that realistically represent the in situ conditions and properties of CPB materials, an apparatus called curing under applied pressure system (CUAPS) was designed and developed at the Université du Québec en Abitibi-Témiscamingue (UQAT). This apparatus was at first intended for examining the UCS development of laboratory-prepared CPB samples cured under equivalent overburden pressure [17,24,45]. CUAPS apparatus was also modified to measure deformation within CPB samples (allowing one-dimensional consolidation testing), pore-water pressure and saturated hydraulic conductivity. The preliminary results illustrate the utility and capacity of the modified CUAPS apparatus in CPB mix recipes optimization for use as underground mine backfill [23,43,46].

The objective of this paper was to assess the effect of some curing conditions (CUAPS-consolidated and mould-unconsolidated) and curing times (7, 14, and 28 days) on microstructural parameters (MIP porosities, pore size distribution, and SSA) and UCS of CPB samples prepared using binder contents of 3, 4.5, and 7 wt.%. The mould-unconsolidated (undrained) samples were cast in conventional plastic moulds and the CUAPS-consolidated (drained) samples were consolidated using the CUAPS apparatus. The MIP parameters (total-, meso- and macro-porosity, threshold diameter, and critical pore size) with UCS results obtained from both CUAPS-consolidated and mould-unconsolidated CPB samples were compared as a function of binder content and curing time. Different empirical relationships were proposed for predicting UCS of CPB samples, knowing certain MIP pore-size distribution parameters.

2. Materials and methods

2.1. Paste backfill ingredients

2.1.1. Mine tailings

Sulphide-rich tailings were obtained from a polymetallic hard rock mine located in the province of Quebec, Canada. Characterization results indicate that the tailings sample has a specific gravity G_s of 3.71 and a specific surface S_m of 2170 m^2/kg. Atterberg limits were determined using an experimental procedure adapted from standard D4318 [41]. Mine tailings showed only slight plasticity, with a liquid limit of 23% and a plastic limit close to zero (Table 1). Similar values have been reported by Bussière [2]. Tailings can be categorized as non-plastic silt (ML) according to the Unified Soil Classification System [42]. Grain size distribution (GSD) of tailings was obtained using a Malvern Laser Mastersizer S2000, and was compared (see Fig. 1) to a typical range of GSD curves for 11 mine tailings from the Quebec and Ontarian mines [15]. Chemical composition of the tailings was analyzed using Inductively Coupled Plasma-Atomic Emission Spectrometry (ICP-AES), model Optima 3100RL and the obtained results were listed in Table 1. Mineralogy of the tailings was obtained by X-ray diffraction (XRD; Bruker AXS D8 Advance Diffractometer) and quantified using the Rietveld method (TOPAS software). The mineralogical composition reveals that tailings sample was composed primarily of pyrite (47.1 wt.%). Significant quantities of silicate minerals such as quartz (31.6 wt.%), chlorite (8.9 wt.%), and paragonite (7.3 wt.%) were detected. More details on mineralogy of the tailings tested can be found in Yilmaz [43].

Table 1
Physico-chemical characteristics of the tailings sample.

Physical properties	Value	Chemical elements (wt.%)	Value
Specific surface area S_s (m^2/kg)	2170	Aluminium Al	2.82
Specific gravity G_s	3.7	Calcium Ca	0.57
Moisture content w (wt.%)	25.12	Silicon Si	0.51
Liquid limit LL (wt.%)	23	Iron Fe	27.42
Effective grain size D_{10} (μm)	4.3	Total sulphur S_{tot}	20.56
Average grain size D_{50} (μm)	24.3	Copper Cu	0.04
Coefficient of uniformity C_u	8	Lead Pb	0.11
Coefficient of curvature C_c	1.1	Zinc Zn	0.35

2.1.2. Hydraulic binders

The hydraulic binder used (OPC–Slag@20:80 wt.%) for CPB preparation was a blend of 80 wt.% blast furnace slag (Slag) and 20 wt.% ordinary Portland cement (OPC). Three binder contents of 3, 4.5, and 7 wt.% were used to produce the CPB mixtures. It is well known that slag exhibits good hardening properties when blended with OPC, as it creates an alkaline environment that activates the slag reaction [44]. However, even when activated by OPC, slag hydration is always slower than that of OPC alone. The chemical composition (by ICP-AES analysis) and some physical properties of the components and the hydraulic binder mixture are given in Table 2. The cement chemistry results show that OPC had a maximum MgO content of 5% and Slag had an Al_2O_3 content lower than 11%. Physical tests show that Slag had the highest BET specific surface at 3540 m^2/kg. OPC alone and the tested hydraulic binder (OPC–Slag@20:80 wt.%) had a BET specific surface of 1580 m^2/kg and 2840 m^2/kg, respectively. The specific gravity of OPC and OPC–Slag@20:80 was 3.1 and 2.8, respectively.

2.1.3. Mixing water

Table 3 summarizes the chemical composition of the as-received tailings interstitial water and mixing water (tap water), analyzed using the ICP-AES method. The as-received tailings interstitial water was highly aggressive, with high sulphate SO_4^{2-} content (4880 ppm). These sulphates were obtained mainly from a cyanide destruction process using SO_2/Air method. Additionally, the high concentration of soluble calcium Ca at 560 ppm is mainly due to the lime added at the ore processing plant. The pH, Eh (redox potential), and EC (electrical conductivity) of the mixing water were analyzed using a Benchtop pH/ISE Meter, Orion Model 920A with a Thermo Orion Triode combination electrode (see Table 3), and were determined at 9.4, +0.15 V, and 7.4 mS/cm for tailings interstitial water and 7.8, +0.43 V, and 0.3 mS/cm for tap water, respectively. Eh was first determined using a Pt/Ag/AgCl electrode and then converted into the standard hydrogen electron potential.

2.2. Sample preparation, mixing, casting, and curing

The required amounts of CPB ingredients (as-received tailings, binding agent, and mixing water) were thoroughly mixed and homogenized in a double spiral concrete mixer for about 7 min to ensure homogeneity of the final paste. Initial water content for all CPB mixes was set at 28.2 wt.% (the equivalent percent solid is 78 wt.%). Water-cement (w/c) ratios of 9.7, 6.5, and 4.3 corresponded to binder proportions of 3, 4.5, and 7 wt.%, respectively. Immediately after mixing, samples were cast in both conventional plastic (non-perforated) moulds and CUAPS Perspex (two open-ended sections) moulds. Both plastic and Perspex moulds had a diameter-to-height (D/H) ratio of 2 ($D \times H$:

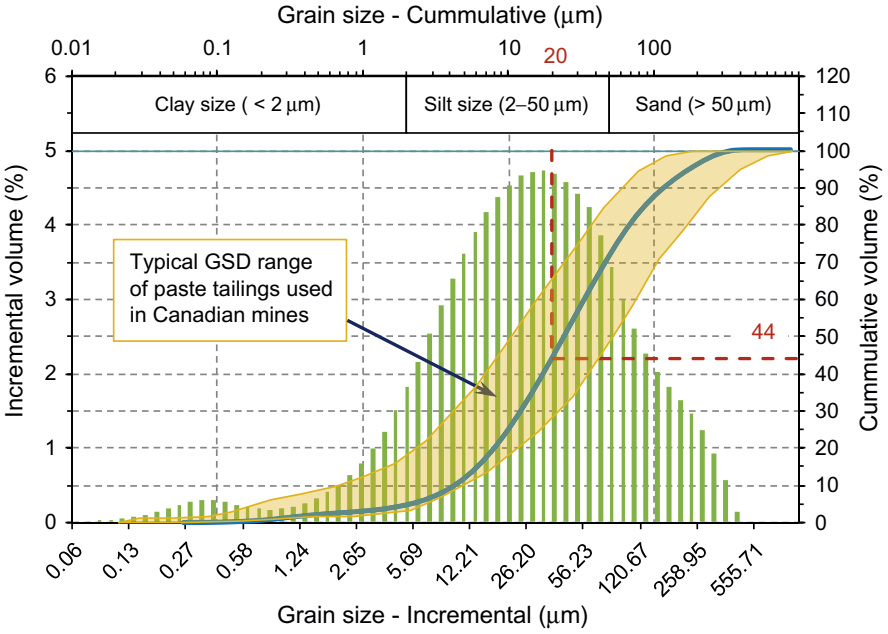

Fig. 1. Grain size distribution (GSD) curves of the mine tailings sample compared to a typical range of GSD curves of 11 tailings sampled from Canadian hard rock mines.

102 × 204 mm). Paste backfills was poured into plastic and Perspex moulds in three layers, each tamped 25 times with an iron rod to remove most of the air pockets within the sample. Initial height was then recorded. Paste backfill cylinders were then sealed and cured for 7, 14, and 28 days in a humidity chamber set at 24 °C and 80% RH to simulate typical curing conditions in underground mines.

2.3. Experimental procedures

2.3.1. Curing under applied pressure tests

To investigate the effects of curing under pressure on the pore structure of CPB materials across curing times, a recently designed laboratory apparatus called CUAPS (curing under applied pressure system) was used [45,46]. The CUAPS apparatus (a total of 10 were used) allows simulating in situ placement properties and curing conditions for laboratory-prepared CPB samples. The CUAPS consists of three main parts: a sample holder (Perspex mould), a pneumatic pressure loading plate equipped with a piston, and a lower plate provided with a drainage port with an outlet for collecting excess pore water. The procedure is as follows. After mounting the backfill sample contained in the Perspex mould, no pressure is applied for the first half an hour, after which pressure is applied and gradually increased to 400 kPa. The final pressure corresponds to an equivalent overburden stress of 17.6 m in height of CPB within an underground stope and having a wet bulk unit weight of 22.7 kN/m^3. Fig. 2 presents photographs of CUAPS-consolidated samples and mould-unconsolidated samples curing in a humidity chamber. A detailed description of the CUAPS apparatus is beyond the scope of this study, but interested readers are referred to Benzaazoua et al. [45], Yilmaz et al. [22–24,40,46] and Yilmaz [43].

2.3.2. Unconfined compression tests

Following curing times of 7, 14, and 28 days, the hardened CPB samples (removed from plastic and Perspex moulds) were subjected to unconfined compression tests (based on ASTM C39 [47] method) to determine UCS using a computer controlled press (MTS 10/GL) with a load capacity of 50 kN and a deformation rate of 1 mm/min. Axial deformation was digitally recorded by a real-time data acquisition system. Observed UCS corresponds to the maximum stress (peak at specimen failure) reached during compressing. For a given CPB recipe, only one test was performed for CUAPS-consolidated samples, whereas three tests were performed on average for mould-unconsolidated samples. However, the reproducibility tests showed reliable and repeatable results across CUAPS apparatuses [24].

2.3.3. Mercury intrusion porosimetry (MIP)

MIP apparatus and test procedure—CPB pore structure network was determined using a mercury intrusion porosimeter (Micromeritics Autopore III 9420). Applying pressures ranging from 0 to 414 MPa (60,000 psi) allows measuring throat pore diameter to 0.003 μm. MIP was analyzed according to ASTM D 4404 [48] standard. After compression testing, representative paste backfill samples weighing between 3.2 and 4.3 g ($D \times H = 12 \times 24$ mm) were taken from locations as far as possible from the shear plane to avoid stress concentration effects that could affect material properties. CPB specimens were oven-dried at 50 °C for at least 96 h and then stored in a dessicator over silica gel to minimize pore alteration due to hydration product destruction and moisture ingress. For a given CPB mixture, two MIP analyses were performed to obtain an average value.

Factors affecting MIP results—MIP results are influenced not only by the microstructure of the specimen, but also by experimental

Table 2
Chemical composition and some physical properties of the binder used.

Parameter	S_m (m^2/kg)	G_s	Al_2O_3 (wt.%)	CaO (wt.%)	Fe_2O_3 (wt.%)	K_2O (wt.%)	MgO (wt.%)	Na_2O (wt.%)	SO_3 (wt.%)	SiO_2 (wt.%)
OPC	1580	3.1	4.86	65.76	2.44	0.83	2.21	2.11	3.67	19.51
Slag	3540	2.8	10.24	31.41	0.55	0.51	11.3	2.01	3.27	36.22
OPC–Slag@20:80	2840	2.9	4.26	42.82	0.64	0.55	6.19	2.03	3.35	30.91

Table 3
Chemical and geochemical analysis of tailings pore water and tap water.

Parameter	As-received tailings pore water	Municipal tap water
Chemical elements		
Aluminium Al (wt.%)	0.212	0.01
Silicon Si (ppm)	0.891	0.901
Magnesium Mg (ppm)	1.83	2.27
Copper Cu (ppm)	0.286	0.835
Iron Fe (wt.%)	0.011	0.066
Calcium Ca (wt.%)	559	40.9
Geochemical parameters		
sulphate content SO_4^{-2} (ppm)	4883	138
Electrical conductivity EC (mS/cm)	7.42	0.274
Corrected redox potential Eh (V)	0.147	0.431
pH (unitless)	9.4	7.8

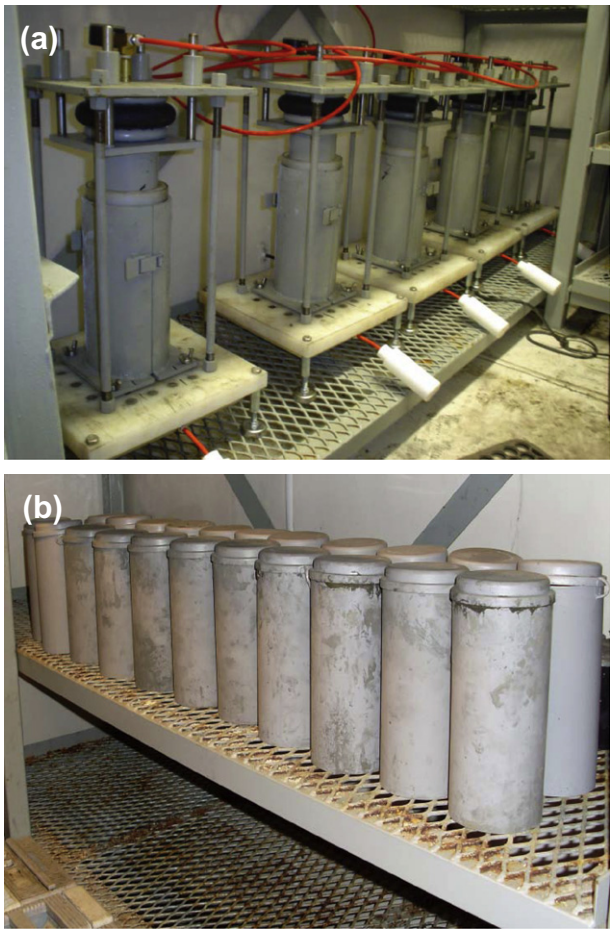

Fig. 2. Photos of (a) CUAPS-consolidated CPB samples and (b) conventional plastic mould-unconsolidated and undrained CPB samples curing in the humidity chamber.

factors such as pre-treatment technique, sample size, pressure build-up rate, pore structure alteration, mercury surface tension, and mercury contact angle [49–51]. In this study, surface tension γ and contact angle φ were taken as 0.485 N/m and 130°, respectively. Based on the International Union of Pure and Applied Chemistry classification [52], there are three pore size categories for cement-based materials: (1) *micropores* are smaller than 0.002 μm, (2) *mesopores* range between 0.002 μm and 0.05 μm and (3) *macropores* are larger than 0.05 μm. MIP tests can measure mesopores and macropores.

2.3.4. Specific surface area determination

For any solid material, specific surface area (SSA or S_m), or the solid total surface area per weight unit (m^2/kg), includes the external geometrical surface as well as the internal surface area [53]. SSA is a good indicator of the fineness of the microstructure. In this study, SSA was determined by measuring nitrogen N_2 multi-point adsorption isotherms based on the BET (Brunauer, Emmett, and Teller) theory according to ASTM D 6556 [54] method. A Gemini III 2375 from Micromeritics was used for surface analysis. Prior to measurement, samples were dried and out-gassed in a Micromeritics VacPrep 061 system at 50 °C for at least 12 h under atmospheric pressure.

3. Results and interpretation

3.1. Effect of curing conditions on pore size distribution and total porosity of CPB

Fig. 3 shows the changes in cumulative and incremental pore size distribution (PSD) curves for 28-day cured CPB samples with binder contents of 3, 4.5, and 7 wt.%. In the PSD curves, MIP total porosity n_{tot} corresponds to the last recorded point (or the highest intrusion pressure and the smallest equivalent pore throat size). Fig. 3a and b show that as binder content increases, pore throat openings become finer due to cementation by binder hydration products and applied pressures during curing. Cumulative PSD curves shift toward smaller average pore diameters with increasing binder proportion. This shift is more evident for CUAPS-consolidated samples than mould-unconsolidated samples, for which cumulative PSD curves are consistently located above those of the consolidated backfills.

Fig. 4 presents the change in average n_{tot} with curing time and binder contents for both mould unconsolidated-undrained and CUAPS-consolidated samples. Consolidated backfill consistently shows lower total porosity n_{tot} and therefore higher bulk density than unconsolidated backfill. Moreover, n_{tot} decreases with increased curing time for mould unconsolidated-undrained and CUAPS-consolidated samples, regardless of binder content. The range of variation in n_{tot} is 39–41% for CUAPS-consolidated samples and 46–47% for mould unconsolidated-undrained CPB samples. Accordingly, curing conditions (with and without applied pressure) appear to play a role in total mercury porosity n_{tot} and PSD of CPB samples for a given binder content.

MIP results are presented in Table 4. Fig. 4 and Table 4 show that total porosity n_{tot} reduces slightly with increased binder content for the two backfill types over the curing time, although the reduction percentage differs across types. Several factors may explain this:

- Fig. 3 shows that the PSD curves depend on both *w/c* ratio (hence UCS, or cohesion) and curing conditions. Thus, Table 5 shows that the *w/c* ratio decreases from its initial value for a given curing time in CUAPS-consolidated CPB samples. The *w/c* ratio of consolidated CPB decreases with the removal of excess water from samples due to the applied pressure during curing and drainage. The reduction in *w/c* ratio is accompanied by a slight reduction in n_{tot}, which could be explained by a reduction in pore size as pores are partially filled by hydrates and/or precipitates (C–S–H gel, gypsum, etc.).
- The effective curing conditions (the combined effects of applied pressure and water drainage on consolidated samples in the CUAPS apparatus) appear to accelerate the cementitious

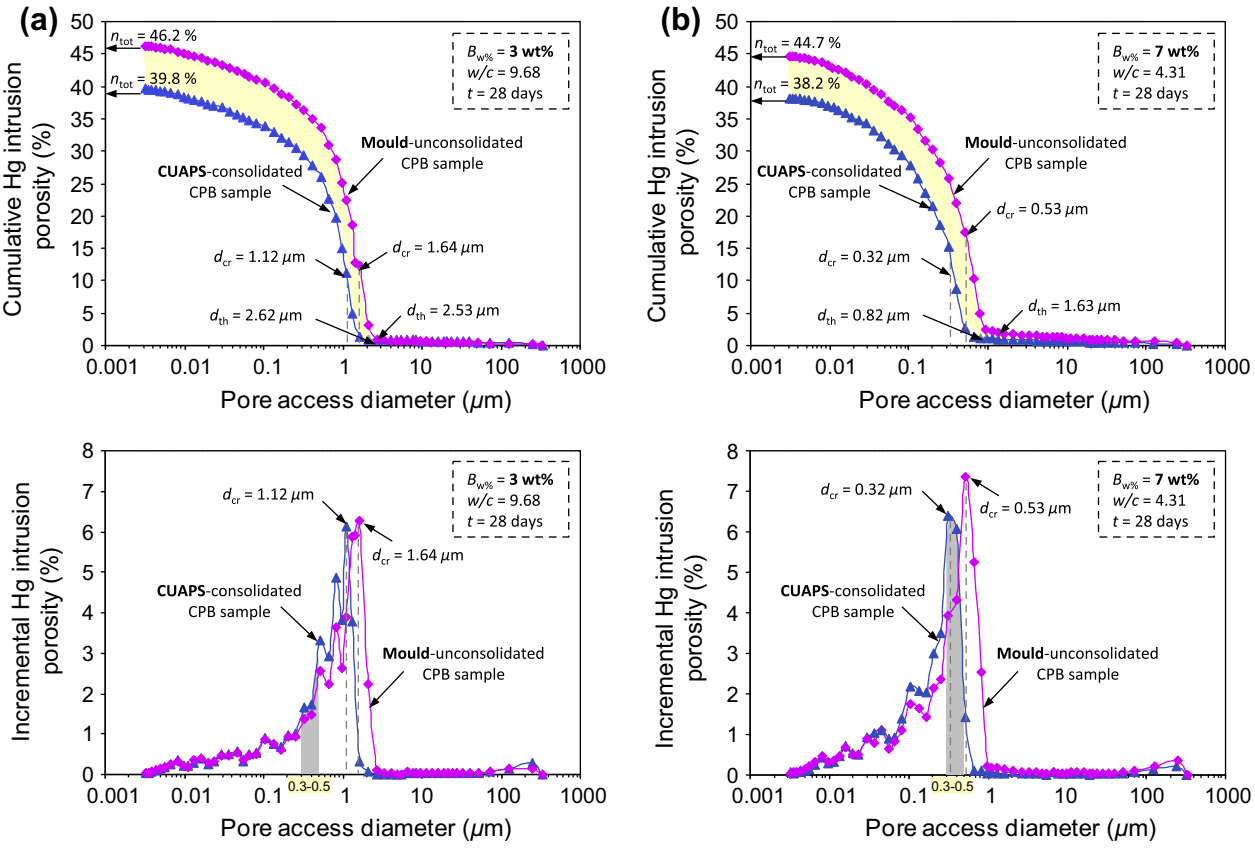

Fig. 3. Effect of different curing conditions (with and without pressure) on pore size distribution (PSD) of CPB samples at 28-days curing for different binder contents: cumulative and incremental PSD curves for (a) $B_{w\%}$ = 3 wt.% and (b) $B_{w\%}$ = 7 wt.%. Shadowed area in the incremental PSD graphs represent total volume in the specific pore range. In this case, the range is between 0.3 and 0.5 μm ($B_{w\%}$ = binder content in wt.%; t = curing time in day).

Table 4
MIP test results for CUAPS-consolidated and mould-unconsolidated CPB samples for different cement contents and curing times.

CPB sample no.	CPB mix no.	Binder content (wt.%)	Curing time (day)	Mesopore[a] porosity n_{meso} (%)	Macropore[b] porosity n_{macro} (%)	Total porosity n_{tot} (%)	Bulk density ρ (g/mL)	Critical pore dia. d_{cr} (μm)	Threshold diameter d_{th} (μm)	Stem[c] volume V_{stem} (%)
CUAPS-consolidated backfill samples										
1	Mix1	3	7	38.6	2.6	41.2	2.13	1.33	2.81	72
2	Mix1	3	14	37.6	3.2	40.8	2.13	1.23	2.74	73
3	Mix1	3	28	35.7	4.1	39.8	2.12	1.12	2.62	76
4	Mix2	4.5	7	37.0	3.3	40.3	2.11	1.13	2.11	75
5	Mix2	4.5	14	34.7	4.7	39.4	2.13	0.82	1.63	76
6	Mix2	4.5	28	33.6	4.8	38.4	2.12	0.53	1.33	73
7	Mix3	7	7	34.9	5.1	40.0	2.09	0.61	0.97	74
8	Mix3	7	14	33.3	5.8	39.1	2.13	0.53	0.92	72
9	Mix3	7	28	32.2	6.0	38.2	2.11	0.32	0.82	74
Mould-unconsolidated backfill samples										
10	Mix1	3	7	44.8	2.6	47.4	1.93	2.17	3.31	72
11	Mix1	3	14	43.0	3.4	46.4	1.90	2.11	2.92	71
12	Mix1	3	28	42.4	3.8	46.2	1.90	1.64	2.53	76
13	Mix2	4.5	7	43.3	3.7	47.0	1.90	1.65	2.71	73
14	Mix2	4.5	14	41.6	4.5	46.1	1.90	1.64	2.53	76
15	Mix2	4.5	28	41.1	4.6	45.8	1.90	1.33	2.21	72
16	Mix3	7	7	40.6	5.2	45.8	1.90	1.33	2.62	73
17	Mix3	7	14	39.5	5.5	45.0	1.90	0.81	2.31	75
18	Mix3	7	28	38.8	5.9	44.7	1.90	0.53	1.63	73

[a] Capillary mesopores range between 0.002 μm and 0.05 μm based on IUPAC classification.
[b] Macropores have pore size larger than 0.05 μm based on IUPAC classification.
[c] Maximum intrusion (stem) volume less than 25% or more than 90% suggests the need for a procedural change. The first instance indicates that a larger sample quantity might give better resolution and the second indicates that the capillary is on the verge of being depleted.

processes through the formation of increasing amounts of cementitious products in a mechanically reduced pore space. However, hydration/precipitation appears to occur to a lesser extent in conventional mould CPB samples that are not allowed to drain. As a result, the porosity of unconsolidated-undrained samples is greater than that of CUAPS-consolidated samples.

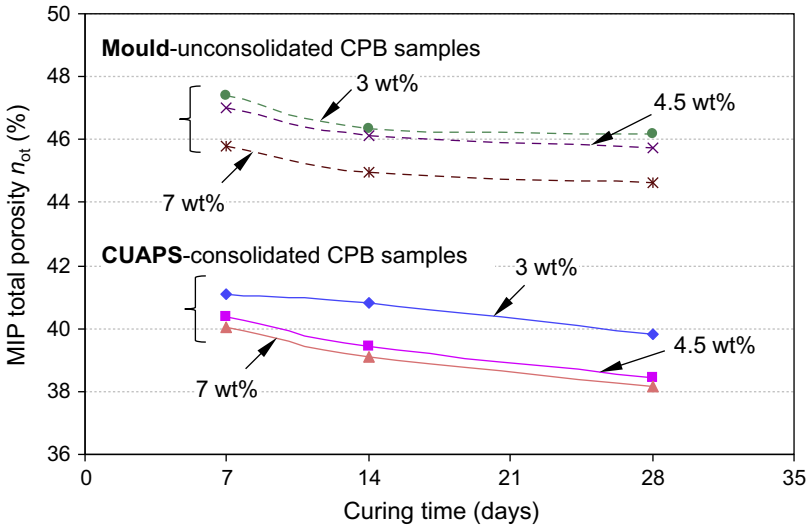

Fig. 4. Change in MIP total porosity with curing time for CUAPS-consolidated and mould-unconsolidated and undrained CPB samples.

Table 5
Calculated final water-to-cement (w/c) ratios of the CPB samples tested for different curing times and binder contents.

Binder content (wt.%)	Initial w/c for all CPB samples	Final w/c for CUAPS-consolidated samples		
		7 days	14 days	28 days
3	9.68	9.07	9.12	9.21
4.5	6.55	6.17	6.19	6.25
7	4.31	4.12	4.13	4.14

The modal distribution of the pore families present in the specimens can be determined from the incremental PSD curves. The graphs in Fig. 3a and b show only one pore family for all CPB sample types. They also show that as binder content increases, the proportion of pores sized 0.3–0.5 μm gradually increases for all samples. Thus, in this pore size range, the incremental porosity for a binder content of 3 wt.% and 7 wt.% are respectively 3.2% and 2.5%, and 6.3% and 4.2% for both CUAPS-consolidated and mould-unconsolidated samples (Fig. 3). Furthermore, by increasing binder content from 3 to 7 wt.%, the maximum incremental mercury porosity (corresponding to critical pore diameter d_{cr}, which can be obtained from the steepest slope of the cumulative PSD curves) increases from 6.1% to 6.4% for consolidated samples, and from 6.3% to 7.4% for unconsolidated samples. From these figures, it is apparent that samples cured under pressure produce greater pore refinement than samples cured traditionally (neither applied pressure nor drainage), mainly due to the accelerated development of cementitious phases.

Figs. 5 and 6 illustrate the change in mesoporosity n_{meso} (pore diameter range is 0.002–0.05 μm) and macroporosity n_{macro} (pore diameter >0.05 μm) for CUAPS-consolidated and mould-undrained CPB samples with binder contents of 3, 4.5, and 7 wt.% after curing for 7, 14, and 28 days. Fig. 5 shows that the n_{meso} of unconsolidated-undrained CPB samples are consistently higher than those of CUAPS-consolidated CPB samples for a given binder content. Overall, n_{meso} decreases slightly with increasing binder content and curing time. For 4.5 wt.% binder, the n_{meso} of CUAPS-consolidated samples decreases from 37% to about 34%, while the n_{meso}

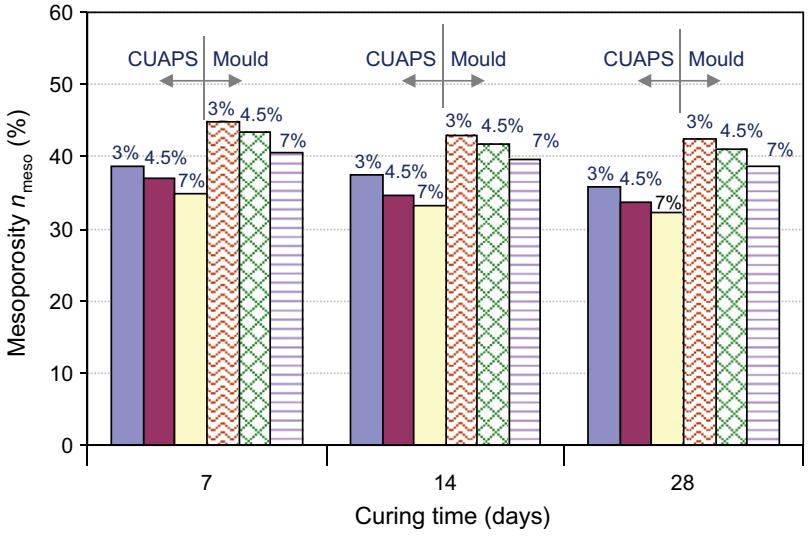

Fig. 5. Change in mesoporosity with curing time for both CUAPS-consolidated and mould-unconsolidated and undrained CPB samples using binder contents of 3, 4.5, and 7 wt.%.

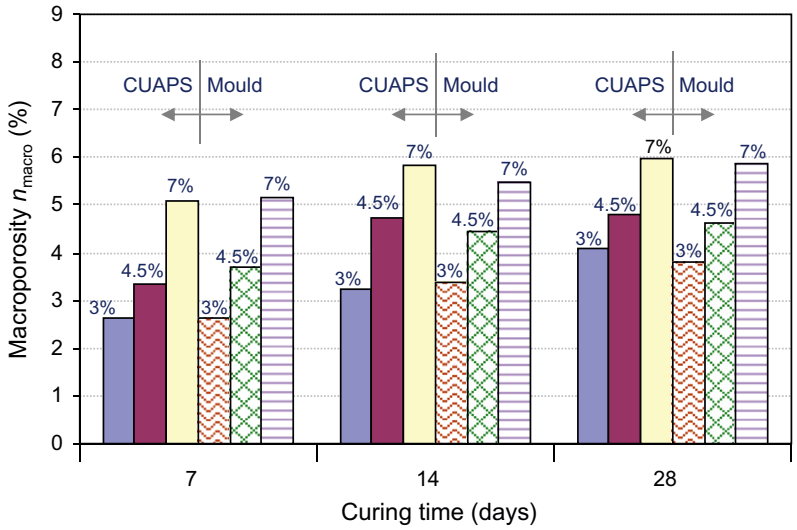

Fig. 6. Change in macroporosity with curing time for both CUAPS-consolidated and mould-unconsolidated and undrained CPB samples using binder contents of 3, 4.5, and 7 wt.%.

of undrained samples decreases from 43% to 41% when curing time increases from 7 to 28 days. Moreover, at early age (7-day curing), n_{meso} for 3, 4.5, and 7 wt.% binders is 39%, 37%, and 35% for CUAPS-consolidated CPB samples, and 45%, 43%, and 41% for unconsolidated-undrained CPB samples. For the same binder contents at 28 days, n_{meso} is 36%, 34%, and 32% for CUAPS-consolidated samples and 42%, 41%, and 39% for unconsolidated-undrained samples. The n_{meso} for CUAPS-consolidated samples decreases at a higher rate (20%) than for undrained samples (15%). The 5% difference could be explained by the CPB skeleton rearrangement due to applied pressure over the curing time (more fine pores and more binder hydrates).

Fig. 6 shows relatively low macroporosity n_{macro} compared to n_{meso} for identical CPB samples under investigation. Changes in n_{macro} are almost the same (mainly a slight increase over time) for both CUAPS-consolidated samples and unconsolidated-undrained samples. For consolidated samples with 3, 4.5, and 7 wt.% binder contents, n_{macro} increases from 2.6% to 4%, 3.3% to 4.8%, and 5% to 6%, respectively when curing time increases from 7 to 28 days. For unconsolidated-undrained samples, n_{macro} increases from 2.6% to 3.8%, 3.7% to 4.6%, and 5.2% to 5.9%, respectively, for 3, 4.5, and 7 wt.% binder contents. However, these results show that macroporosity is less affected than mesoporosity by applied pressure.

3.2. Effect of curing conditions on critical pore size and threshold diameter of CPB

Other parameters can be used to characterize the pore structure of a cement-based material, such as critical pore size d_{cr} and threshold diameter d_{th} [55]. Critical pore size (or maximum continuous pore size) corresponds to the steepest slope of the cumulative porosity curve. The highest point of the steepest slope represents the mean size of pore entryways that allows maximum percolation throughout the pore system. The critical pore size d_{cr} controls the transmissivity of the material, and this parameter is most often used to examine the effect of factors such as *w/c* ratio, curing conditions, and time on pore structure change. The threshold diameter

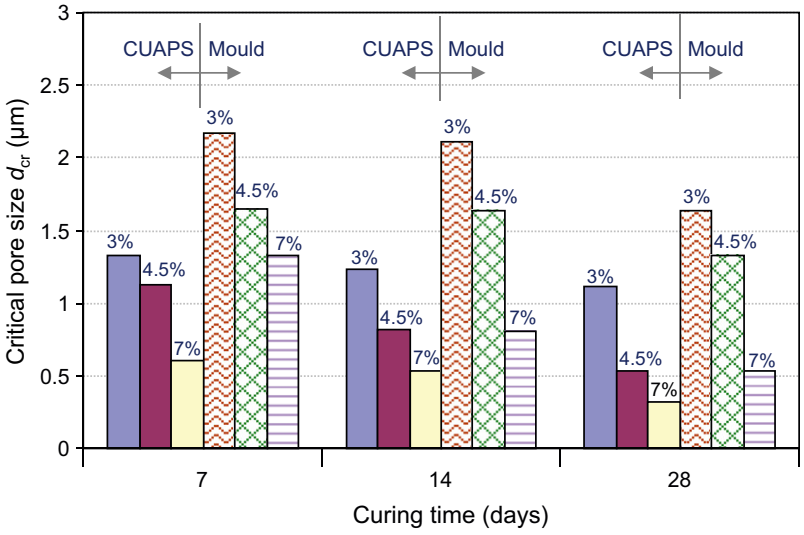

Fig. 7. Change in critical pore diameter with curing time for both CUAPS-consolidated and mould-unconsolidated and undrained CPB samples using binder contents of 3, 4.5, and 7 wt.%.

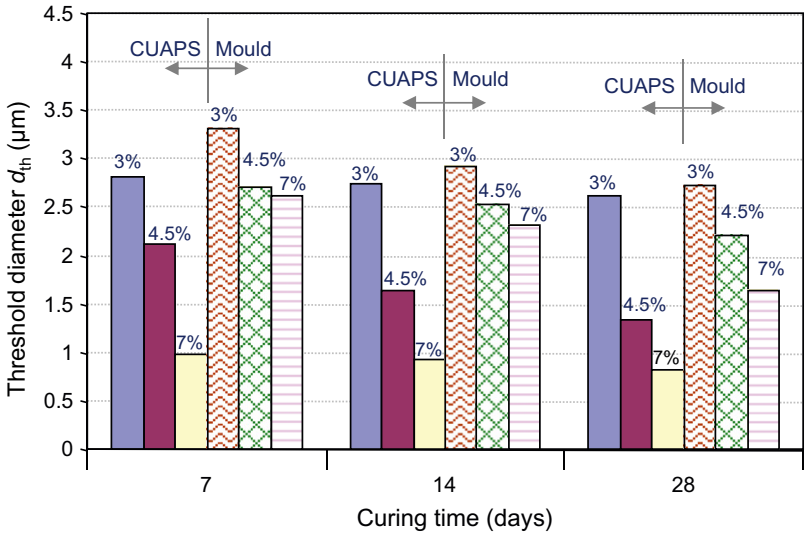

Fig. 8. Change in threshold diameter with curing time for both CUAPS-consolidated and mould-unconsolidated and undrained CPB samples using binder contents of 3, 4.5, and 7 wt.%.

is the largest pore diameter at which significant intruded pore volume is detected and the mercury begins to penetrate into the pores of samples. All PSD curves display a threshold diameter d_{th} above which there is comparatively little mercury intrusion and immediately below which most intrusion begins [56].

Fig. 7 shows the change in d_{cr} with curing time for both mould-undrained and CUAPS-consolidated samples. As can be seen, d_{cr} decreases with increased binder content (3–7 wt.%) and slightly decreases with curing time. Consolidated samples produce lower d_{cr} than mould-undrained samples. For 4.5 wt.% binder content, d_{cr} at curing times of 7, 14, and 28 days is respectively 1.13 μm, 0.82 μm, and 0.53 μm for CUAPS-consolidated samples, and 1.65 μm, 1.64 μm, and 1.33 μm for mould-undrained samples (see Table 4).

Fig. 8 shows that d_{th} decreases with increased binder content (3–7 wt.%) and decreases slightly over curing time (7–28 days). After 28-day curing and for binder contents of 3, 4.5, and 7 wt.%, consolidated samples show lower d_{th} at 2.62 μm, 1.33 μm, and 0.82 μm than unconsolidated-undrained samples at 2.53 μm, 2.21 μm, and 1.63 μm, respectively. For the highest binder (7%), d_{th} for undrained samples is respectively 2.62 μm, 2.31 μm, and 1.63 μm for curing times of 7, 14, and 28 days. For consolidated samples, d_{th} is respectively 0.97 μm, 0.92 μm, and 0.82 μm, corresponding to a decrease of 170%, 151%, and 99% after 7, 14, and 28 days of curing. This confirms that curing under pressure contributes to refine the microstructure of hardened CPB mass. Pores constrict during the curing process as precipitation/hydration phenomena happening in the pores progresses. Hence, d_{th} values lessen as curing time increases and *w/c* ratio decreases, as reported by various authors [35,38,57]. In summary, MIP results show that threshold diameter ranges from 3.31 μm to 0.82 μm, which is fairly similar to the findings of Ouellet et al. [35].

3.3. Effect of curing conditions on compressive strength development of CPB

Fig. 9 shows the change in unconfined compressive strength (UCS) of CUAPS-consolidated samples and mould unconsolidated-

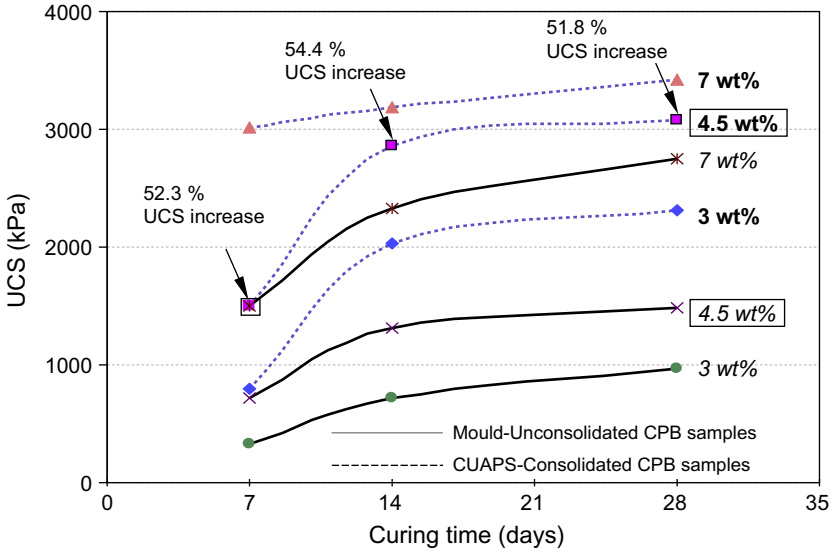

Fig. 9. Change in unconfined compressive strength (UCS) with curing time for mould-unconsolidated and undrained and CUAPS-consolidated CPB samples.

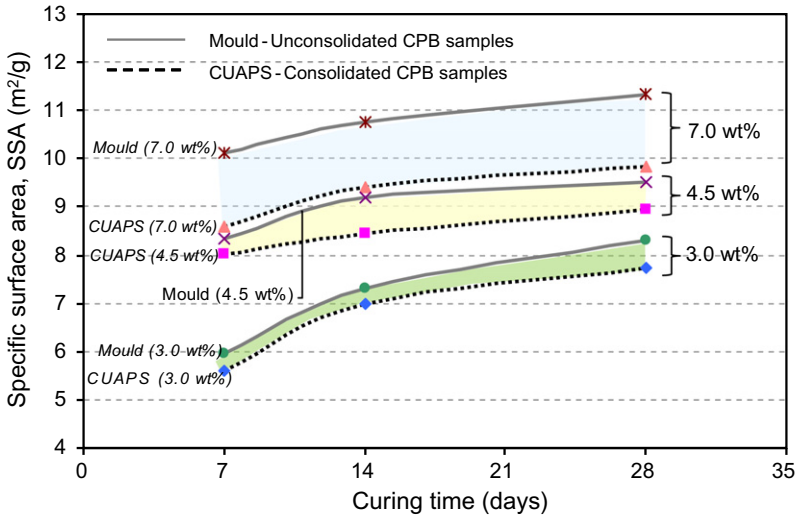

Fig. 10. Change in specific surface area (SSA) with curing time for mould-unconsolidated and undrained and CUAPS-consolidated CPB samples using binder contents of 3, 4.5, and 7 wt.%. Coloured areas in the graph represent the difference observed between CUAPS-consolidated CPB and mould-unconsolidated CPB. (For interpretation of the references to colour in this figure legend, the reader is referred to the web version of this article.)

undrained samples with curing time. It is apparent that curing conditions (with and without applied pressure) impact the compressive strength development of CPB samples. Consolidated samples always produce higher UCS than unconsolidated-undrained samples for a given binder content. In comparison, the UCS of CUAPS-consolidated samples having a binder content of 3 wt.% is respectively 57.9%, 64.3%, and 58.2% higher than that of unconsolidated-undrained samples for curing times of 7, 14, and 28 days. With binder contents of 4.5 and 7 wt.%, UCS is 52.3%, 54.4%, and 51.8% higher, and 50.5%, 27.1%, and 19.8% higher, respectively. The higher UCS for consolidated CPB samples can be explained by the combined effects of applied consolidation pressures during curing and the removal of excess water, which accelerates the binding reaction, thereby producing higher UCS.

Previous works [7,12,13,17,24,31,37,58] have pointed out that the drainage of excess water within the backfill positively affects binder hydration. As hydration progresses, the resulting cement products intrude into the CPB pore space (i.e., pore sizes become smaller), producing higher strength. Therefore, increased curing time and decreased *w/c* ratio result in lower porosity (see Table 5). In addition, some phases (such as sulphates) could have reached saturation more easily, as lower water contents were observed in the consolidated CPB samples, and no (or negligible) cement species were lost during drainage [12]. This would lead to more dense cementitious matrices (i.e., pore spaces were filled with cementitious phases), which in turn led to better cohesion. The hardening process of CPB during curing is addressed elsewhere [7].

3.4. Effect of curing conditions on specific surface area of CPB

Fig. 10 shows the change in SSA for CUAPS-consolidated samples and mould unconsolidated-undrained samples with curing time. Overall, SSA increases with increasing binder content and curing time. For 3 wt.% binder content, SSA values are 5594, 6981, and 7729 m^2/kg for consolidated samples and 5967, 7320, and 8297 m^2/kg for unconsolidated-undrained samples for curing times of 7, 14, and 28 days, respectively. For 7 wt.% binder content, SSA values are 8590, 9418, and 9826 m^2/kg for CUAPS-consolidated samples and 10,120, 10,748, and 11,327 m^2/kg for mould-unconsolidated samples. Overall, unconsolidated CPB samples consistently produce higher SSA than consolidated samples for a given binder content and curing time, confirming previous findings by Belem et al. [19]. Moreover, after 28 days, as binder content increases from 3 to 7 wt.%, SSA increases from 7729 to 9826 m^2/kg for consolidated CPB samples and from 8297 to 11,327 m^2/kg for unconsolidated-undrained CPB samples. This significant increase in material fineness can be partly explained by the gradual formation of cement hydration products. These observations are also supported by earlier SSA tests performed on unconsolidated backfills cured for 91 days [59].

4. Relationship between compressive strength and microstructural parameters

The microstructure of CPB samples is directly related to their physical and mechanical properties [55]. Among the factors determining the UCS of a cementitious material are (i) the chemistry of binder and the tailings GSD, (ii) the water-to-cement ratio *w/c* of CPB, (iii) mixing conditions, and (iv) curing conditions, especially RH, temperature, and time [60]. UCS is the most often used index parameter for CPB mix optimization and stability design. Thus, it is particularly relevant to evaluate how this index parameter is affected by changes in the pore structure of hardened CPB.

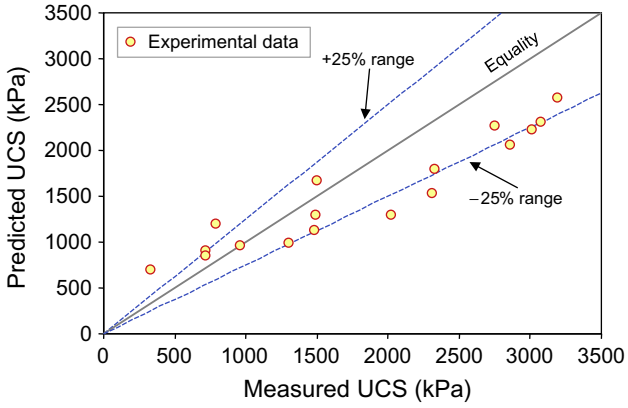

Fig. 11. Comparison of laboratory measured and predicted UCS values using Eq. (1) with the MIP total and partial porosity data obtained from the present study.

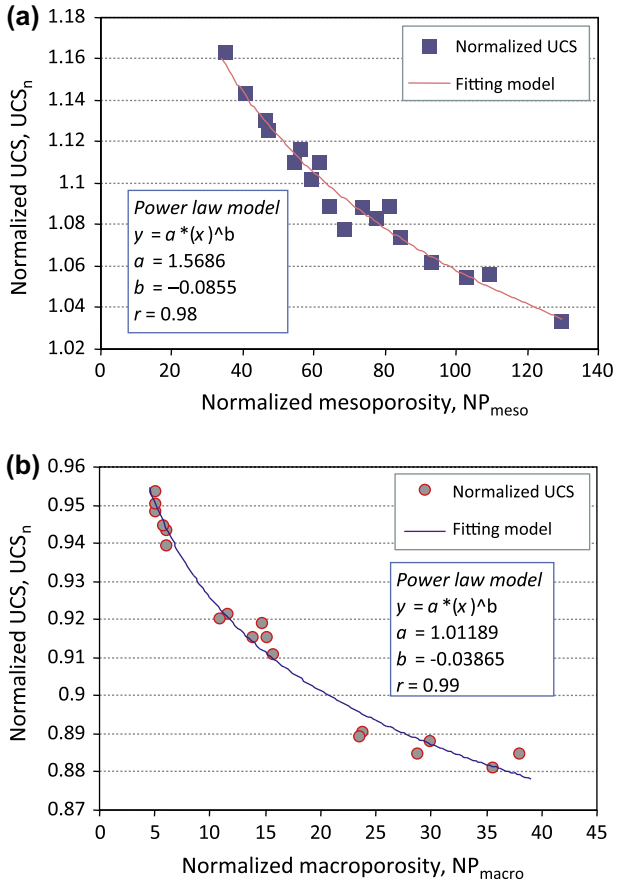

Fig. 12. Graphical representation of Eq. (2) showing the relationship between (a) normalized UCS *vs.* normalized mesoporosity and (b) normalized UCS *vs.* normalized macroporosity of CPB samples.

Many attempts have been made to express the empirical and semi-analytical relationships between the UCS and porosity of different types of cement-based materials such as cement pastes, concrete, mortars, and CPB [35,36,61–67]. These studies showed that UCS development within cement-based material is a function of the number, shape, and distribution of the void space and porosity. It is generally accepted that the relationship between strength and porosity can be simply and empirically represented by a linear plot [68]. Nevertheless, nonlinear regression correlations using exponential, power law and yield-density models are also commonly used. A number of relationships between UCS and porosity are found in the literature for a given material. Some of these relations use total porosity $n_{\text{Hg-tot}}$ while others use fractional pore size or partial porosity derived from MIP cumulative PSD curves. Most relationships also use strength at zero porosity and/or porosity at zero strength parameters, which can be difficult to estimate [69].

Ouellet et al. [35] proposed a generalized power law model that distinguishes between the contribution of total porosity and size-dependent porosity (based on $d = 0.3$ μm pore size) for CPB materials. The proposed predictive equation (Eq. (1)), in which the effect of microstructural evolution is evaluated by two fractional size distributions (fine and coarse pore sizes) based on the fixed diameter $d = 0.3$ μm, is given as follows:

$$\sigma_{cn} = \sigma_{n_{min}} \left[\frac{(1-n)}{(1-n_{min})}\right]^{u} \cdot \left[\frac{(1-n_{\geqslant d})}{(1-n_{<d})}\right]^{V} \quad (1)$$

where σ_{cn} is the unconfined compressive strength UCS (kPa) for a given MIP total porosity n, σ_{nmin} is the reference compressive strength UCS at minimum porosity n_{min}, $n_{\geqslant d}$ is the cumulative MIP porosity for pore sizes larger than diameter d (=0.3 μm), $n_{<d}$ is the cumulative MIP porosity for pore sizes smaller than diameter d, and u and V are exponents used to define the non-linearity of the two functions in brackets.

The model was developed based on UCS data obtained from CPB samples prepared with OPC and blended binders and cast in standard plastic moulds. More details on the CPB recipes tested to develop Eq. (1) can be found in Ouellet et al. [35]. Eq. (1) implies that the UCS is related to the difference between MIP total porosity and minimum porosity (first term of Eq. (1)) and to the ratio of pore fraction greater than 0.3 μm and the fraction lower than 0.3 μm. Based on their data, in which no significant change in MIP total porosity was observed for all specimens tested, Ouellet et al. [35] suggested values of 1 and 5.2 for the u and V exponents, while mentioning that these two parameters were obtained by fitting.

To obtain the best fit between the results obtained in the present study using Eq. (1), parameter u was set equal to 1, while parameter V was changed to 3.2. A possible explanation for the need to slightly reduce the value of exponent $V = 5.2$ would be the differences in tailings mineralogy and GSD, mixing water geochemistry, binder types, and their proportions and curing conditions (consolidated or unconsolidated). Fig. 11 presents experimental UCS data compared to calculated UCS values using Eq. (1), showing that about 80% of the experimental UCS data are predicted within a precision range of ±25%. Considering that this predictive equation is usually used for preliminary assessment of UCS when only small amounts of material are available, the precision obtained with Eq. (1) can be considered acceptable. However, this predictive equation could not replace a proper experimental determination of UCS of CPB materials for purposes of design or quality control monitoring.

4.1. Proposed correlations between UCS and MIP parameters for CPB

In the following subsections, some empirical relationships, based on microstructural parameters (mesoporosity, macroporosity, total porosity, threshold diameter and specific surface area) and UCS are proposed using regression (best fit) analyses.

4.1.1. Correlations between UCS and mesoporosity and macroporosity

The pore system in cement-based materials consists mainly of three pore types: gel *micropores* (pores within the C–S–H gel or hydrated products), capillary *mesopores* (residual pores from cement hydration), and larger *macropores* [52]. Kendall et al. [61] demonstrated that gel pores are too small to initiate cracking

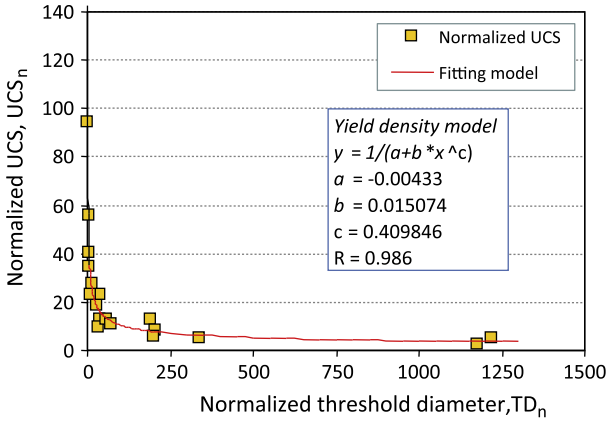

Fig. 13. Graphical representation of Eq. (3) showing the relationship between normalized UCS and normalized threshold diameter for CPB samples.

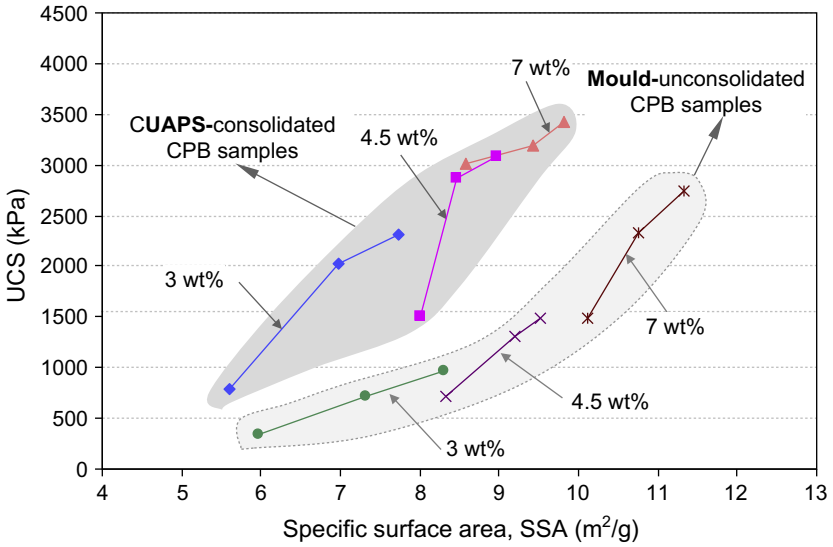

Fig. 14. Change in unconfined compressive strength UCS with specific surface area SSA for all CPB samples.

under relatively low stress, and therefore do not detract from the compressive strength of cement-based material. Capillary pores and other larger pores, however, are responsible for reductions in strength and elasticity [57,60,70]. Capillary pores are therefore sufficient to initiate cracking, hence reducing the UCS gain of cemented-based materials [61]. Therefore, the pore structure considered here are *mesopores* (between 0.002 μm and 0.05 μm) and *macropores* (larger than 0.05 μm).

Fig. 12a and b illustrate the fitted power law relationship of normalized UCS [$UCS_n = y = (UCS * B_{w\%})^{\beta_1}/(t)^{\beta_2}$] as a function of normalized mesoporosity ($x = NP_{meso}$)/macroporosity ($x = NP_{macro}$) [$x = n_{meso,macro} * (t/B_{w\%})^{\beta_0}$] for the combined data obtained from CUAPS-consolidated and mould-unconsolidated CPB samples. Substituting the normalized variables into a power law relationship [$y = a * x\hat{}b$] yields the empirical relationship between UCS and n_{meso} or n_{macro}, given in Eq. (2) as follows:

$$UCS = \alpha \cdot (n_{meso,macro})^{\beta_0} \cdot \frac{t^{\beta_1}}{(B_{w\%})^{\beta_2}} \quad (2)$$

where UCS is the unconfined compressive strength (kPa), $n_{meso,macro}$ is the meso- or macro-porosity (%), t is the curing time (days), $B_{w\%}$ is the binder content (wt.%), and α, β_0, β_1, and β_2 are empirical constants. For the binder used (OPC–Slag@20:80), $\alpha = 6.62E{+}07$, $\beta_0 = -3.4201$, $\beta_1 = 0.29$, and $\beta_2 = -0.71$ for n_{meso}, and $\alpha = 10.6528$, $\beta_0 = -7.7293$, $\beta_1 = 2.2706$, and $\beta_2 = -6.7293$ for n_{macro}, with a coefficient of correlation $r = 0.98$ (n_{meso}) and $r = 0.99$ (n_{macro}), respectively. This equation can be used for other binder types simply by adjusting the fitting constants.

4.1.2. Correlation between UCS and threshold diameter

Diamond [56] suggested that, due to limitations in the interpretation of MIP results, the effective diameter d_{eff} or threshold diameter d_{th} should be used to compare pore structures of cement-based materials. In this view, Fig. 13 presents a general yield-density fitting relationship of normalized UCS [$UCS_n = y = (UCS * B_{w\%})^{k_1}/(t)^{k_2}$] as a function of normalized threshold diameter [$TD_n = x = d_{th} * (t/B_{w\%})^{k_0}$] for the combined data obtained from CUAPS-consolidated and mould-unconsolidated CPB samples. This figure shows that as d_{th} decreases, UCS increases. Substituting the normalized variables into a yield-density model [$y = 1/(a + b * x\hat{}c)$] yields the empirical relationships between UCS and d_{th}, given in Eq. (3) as follows:

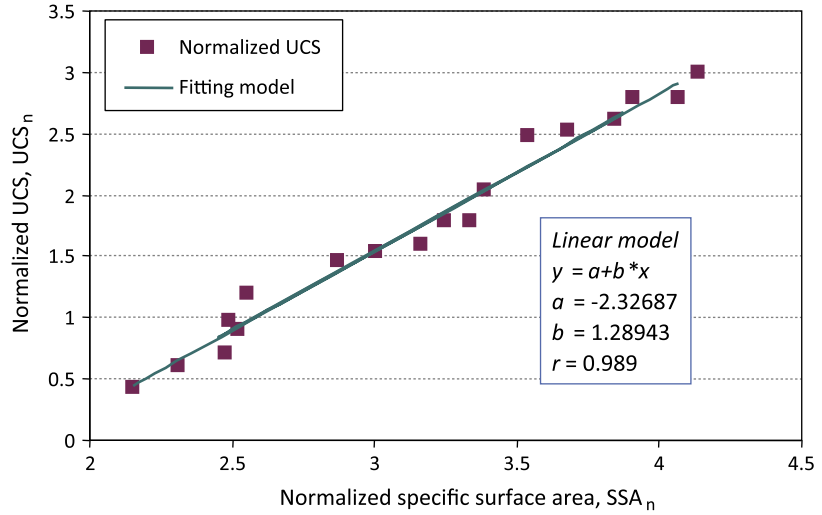

Fig. 15. Graphical representation of Eq. (4) showing the relationship between normalized UCS and normalized SSA for CPB samples.

$$\mathrm{UCS} = \frac{(t)^{\alpha_0}}{B_{w\%}\left(a + b\cdot(d_{th})^{c}\cdot\left(\frac{t}{B_{w\%}}\right)^{\alpha_1}\right)^{\alpha_2}} \quad (3)$$

where UCS is the unconfined compressive strength (kPa), d_{th} is the threshold diameter (μm), t is the curing time (days), $B_{w\%}$ is the binder content (wt.%), and α_0, α_1, α_2, a, b, and c are empirical constants. For the binder type used (OPC–Slag@20:80), $\alpha_0 = 2$, $\alpha_1 = 1.1270$, $\alpha_2 = 1.3333$, $a = -0.0043$, $b = 0.015$, and $c = 0.4098$, with a coefficient of correlation $r = 0.99$. Again, this equation can be used for other CPB types by adapting the fitting constants.

4.1.3. Correlation between UCS and specific surface area SSA

Specific surface area (SSA or S_m), which is a fineness parameter, provides indirect information about the microstructure of CPB samples during curing. Therefore, SSA can be closely related to the UCS development of CPB materials [19,20,59]. Fig. 14 shows the change in UCS for both CUAPS-consolidated and mould-unconsolidated CPB samples as a function of SSA, indicating proportionality between SSA and the binder content used within CPB, and therefore UCS development. It is generally accepted that increasing the fineness of cement particles can increase the hydration rate. Hence, increasing the hydration rate also increases the degree of hydration, which in turn produces higher strength development. However, it is observed from Fig. 14 that SSA is not the only parameter that controls strength development. In fact, consolidated backfills often show higher UCS and surprisingly lower SSA than unconsolidated backfills for a given binder content. This unexpected observation is probably due to the combined effects of the formation of precipitated cement hydrates and the particle rearrangement process at the early stages of compaction (removal of water leads to solid density increase or decrease in the voids present within the CPB material).

Fig. 15 presents a fitted linear relationship of the normalized UCS [$\mathrm{UCS}_n = y = \ln[(\mathrm{UCS} * B_{w\%})^{k_1}/(t)^{k_2}]$] as a function of normalized SSA [$\mathrm{SSA}_n = x = \ln[\mathrm{SSA} * (t/B_{w\%})^{k_0}]$] for the combined data obtained from CUAPS-consolidated and mould-unconsolidated CPB samples. This figure shows that as normalized SSA increases, UCS increases proportionally. Substituting the normalized variables into a linear model [$y = a + b * x$] yields the empirical relationships between compressive strength (UCS) and specific surface area (SSA), given in Eq. (4) as follows:

$$\mathrm{UCS} = \lambda\cdot(\mathrm{SSA})^{\alpha}\cdot(B_{w\%})^{\beta_0}t^{\beta_1} \quad (4)$$

where UCS is the unconfined compressive strength (kPa), SSA is the specific surface area (m^2/g), t is the curing time (days), $B_{w\%}$ is the binder content (wt.%), and λ, α, β_0, and β_1 are empirical constants. For the binder type used (OPC–Slag@20:80), $\lambda = 9.074\mathrm{E}{-05}$, $\alpha = 5.1577$, $\beta_0 = -5.6677$, and $\beta_1 = -1.3322$, with a coefficient of correlation $r = 0.99$. This equation can be used for other CPB types by adapting the fitting constants.

5. Conclusions

This paper presents the results of an experimental investigation of the microstructure of different mixtures of cemented paste backfill (CPB) samples (binder contents of 3, 4.5, and 7 wt.%) characterized by mercury intrusion porosimetry (MIP) and specific surface area (SSA) measurement. Two types of backfill samples, CUAPS-consolidated (using a recently developed and improved consolidometer = CUAPS apparatus = Curing Under Applied Pressure System) and mould-unconsolidated CPB samples were prepared. Total porosity n_{tot}, pore size distribution PSD, threshold diameter d_{th}, and compressive strength UCS of the CPB samples were determined for 3, 4.5, and 7 wt.% binder contents and after 7, 14, and 28-day curing times. Based on the obtained results, the following conclusions can be drawn:

- MIP total porosity n_{tot} decreased from 41% to 38% for CUAPS-consolidated backfills and from 47% to 45% for mould-unconsolidated backfills, depending on the w/c ratio and curing time. Longer curing times and lower w/c ratios therefore result in lower total porosity values.
- Binder content and curing time play a significant role in resultant CPB pore size distribution (PSD). Increased binder content (from 3 to 7 wt.%) caused PSD curves to shift towards lower pore size, resulting in decreased porosity and threshold diameters.
- Threshold diameter d_{th} of CUAPS-consolidation backfills ranged from 2.81 μm to 0.82 μm while d_{th} of mould-unconsolidated backfills ranged from 3.31 μm to 1.63 μm. For a given CPB, longer curing times (up to 28 days) and lower w/c ratios therefore result in lower threshold diameter.
- UCS data reveal that CUAPS-consolidated backfills consistently produced higher strength than mould-unconsolidated backfills, mainly due to the consolidation that refines the pore structure during curing. A clear relationship was found between MIP pore-size parameters ($d < 0.3$ μm, mesoporosity and macroporosity) and unconfined compressive strength UCS. The resulting empirical predictive equations can be used for preliminary assessment of CPB compressive strength.
- From the SSA data, it was inferred that specific surface was indirectly related to the UCS development for each CPB specimen. This implies that the greater the SSA, the higher the volume of cement hydration products (for mould-unconsolidated samples), resulting in considerably increased strength of CPB. An empirical predictive model of UCS based on SSA data of CPB was proposed and can be used for preliminary assessment of UCS values.

Acknowledgements

The authors would like to express their appreciation to the NSERC Discovery Grant Program, the Industrial NSERC-Polytechnique-UQAT Chair in Environment and Mine Wastes Management, and the Canadian Research Chair in Integrated Mine Waste Management for their generous financial support during the research. The Canada Foundation for Innovation (CFI) is also gratefully acknowledged for the manufacture of the ten CUAPS apparatuses. Special thanks are extended to Pierre Trudel of G+ Plus Industrial Plastic Inc. for his collaborative assistance in modifying the CUAPS apparatus, to David Bouchard, Yvan Poirier, and Nil Gaudet (UQAT-URSTM technicians) for their technical support, to Nathan Mutch of Lafarge North America Inc. for kindly providing the cement materials, and to Dr. Serge Ouellet of Agnico-Eagle Mines Limited (Technical Services Division).

References

[1] Potvin Y, Thomas EH, Fourie AB. Handbook on mine fill. Perth, Western Australia, Australia: Australian Centre for Geomechanics Publication; 2005.
[2] Bussière B. Colloquium 2004: hydrogeotechnical properties of hard rock tailings from metal mines and emerging geoenvironmental disposal approaches. Can Geotech J 2007;44(9):1019–52.
[3] Belem T, Benzaazoua M. Design and application of underground mine paste backfill technology. Geotech Geol Eng 2007;26(2):147–74.
[4] Belem T, Benzaazoua M. Predictive models for pre-feasibility cemented paste backfill mix design. In: The 3rd international conference on post-mining'08, February, 6–8, vol. 1–13, Nancy, France; 2008. p. 155–69.
[5] Benzaazoua M, Ouellet J, Servant S, Newman P, Verburg R. Cementitious backfill with high sulfur content: physical, chemical and mineralogical characterization. Cem Concr Res 1999;29(5):719–25.

[6] Benzaazoua M, Belem T, Bussière B. Chemical factors that influence the performance of mine sulphidic paste backfill. Cem Concr Res 2002;32(7):1133–44.
[7] Benzaazoua M, Fall M, Belem T. A contribution to understanding the hardening process of cemented pastefill. Miner Eng 2004;17(2):141–52.
[8] Kesimal A, Ercikdi B, Yilmaz E. The effect of desliming by sedimentation on paste backfill performance. Miner Eng 2003;16(10):1009–11.
[9] Kesimal A, Yilmaz E, Ercikdi B. Evaluation of paste backfill mixtures consisting of sulphide-rich mill tailings and varying cement contents. Cem Concr Res 2004;34(10):1817–22.
[10] Kesimal A, Yilmaz E, Ercikdi B, Alp I, Deveci H. Effect of properties of tailings and binder on the short and long terms strength and stability of cemented paste backfill. Mater Lett 2005;59(28):3703–09.
[11] Belem T, Benzaazoua M, Bussière B. Mechanical behaviour of cemented paste backfill. In: The 53rd canadian geotechnical conference geotechnical engineering at the dawn of the third millennium, vol. 1, Montreal, Quebec, Canada; October 15–18, 2000. p. 373–80.
[12] Belem T, El Aatar O, Benzaazoua M, Bussière B, Yilmaz E. Hydro-geotechnical and geochemical characterization of column consolidated cemented paste backfill. In: The 9th international symposium in mining with backfill, CIM, Montreal, Quebec, Canada; April 29–May 2, 2007. p. 162–71.
[13] Fall M, Benzaazoua M, Ouellet S. Experimental characterization of the influence of tailings fineness and density on the quality of cemented paste backfill. Miner Eng 2005;18(1):41–4.
[14] Godbout J. Évolution des propriétés hydriques des remblais miniers cimentés en pâte durant le curage. MSc Thesis. École Polytechnique de Montréal, Québec, Canada; 2005.
[15] Ouellet S. Mineralogical characterization, microstructural evolution and environmental behaviour of mine sulphidic cemented paste backfills. Ph.D. Thesis. Université du Québec en Abitibi-Témiscamingue, Rouyn-Noranda, Québec, Canada; 2006.
[16] Yilmaz E, Belem T, Benzaazoua M, Kesimal A, Ercikdi B. Evaluation of the strength properties of deslimed tailings paste backfill. Miner Resource Eng 2007;12(2):129–44.
[17] Yilmaz E, Belem T, Benzaazoua M, Bussiere B. Experimental characterization of the influence of curing under stress on the hydromechanical and geotechnical properties of cemented paste backfill. In: The 12th international conference on tailings and mine waste, Vail, Forth Collins, Colorado, USA; October 18–23, 2008a. p. 139–52.
[18] Ercikdi B, Kesimal A, Cihangir F, Deveci H, Alp I. Cemented paste backfill of sulphide-rich tailings: importance of binder type. Cem Concr Compos 2009;31(4):268–74.
[19] Belem T, Benzaazoua M, Bussière B, Dagenais AM. Effects of settlement and drainage on strength development within mine paste backfill. In: The 9th international conference on tailings and mine waste, Vail, Forth Collins, Colorado, USA, Balkema; January 27–30, 2002. p. 139–48.
[20] Belem T, El Aatar O, Bussière B, Benzaazoua M, Fall M, Yilmaz E. Characterization of self-weight consolidated paste backfill. In: The 9th international seminar on paste and thickened tailings, Limerick, Ireland; April 3–7, 2006. p. 333–45.
[21] le Roux K. In situ properties and liquefaction analysis of cemented paste backfill. Ph.D. Thesis. The University of Toronto, Toronto, Ontario, Canada; 2004.
[22] Yilmaz E, El Aatar O, Belem T, Benzaazoua M, Bussiere B. Effect of consolidation on the performance of cemented paste backfill. In: The 21st underground mine support conference, Val d'Or, Quebec, Canada; April 11–12, 2006. p. 1–14.
[23] Yilmaz E, Belem T, Bussiere B, Benzaazoua M. Consolidation characteristics of early age cemented paste backfill. In: 61st Canadian geotechnical conference, Edmonton, Alberta, Canada; September 21–24, 2008b. p. 797–804.
[24] Yilmaz E, Benzaazoua M, Belem T, Bussière B. Effect of curing under pressure on compressive strength development of cemented paste backfill. Miner Eng 2009;22(9-10):772–85.
[25] Fourie AB, Fahey H, Helinski M. Using effective stress theory to characterize the behaviour of backfill. CIM Bull 2007;100(1103):1–9 (Paper 27).
[26] Grabinsky MW, Bawden FW. In situ measurements for geomechanical design of cemented paste backfill systems. CIM Bull 2007;100(1103):1–8 (Paper 21).
[27] El Aatar O. Consolidation behavior of cemented paste backfill material. M.Sc. Thesis. Université du Québec en Abitibi-Témiscamingue (UQAT), Rouyn-Noranda, Québec, Canada; 2009.
[28] Helinski M, Fourie AB, Fahey M. Mechanics of early age cemented paste backfill. In: The 9th international seminar on paste and thickened tailings, Limerick, Ireland; April 3–7, 2006. p. 313–22.
[29] Helinski M, Fourie AB, Fahey M. Preliminary results from an investigation into the effect of application of effective stress to cemented paste backfill during curing. ACG Newslett 2009;31(12):10–3.
[30] Garboczi EJ. Permeability, diffusivity, and microstructural parameters: a critical review. Cem Concr Res 1990;20(4):591–601.
[31] Belem T, Bussière B, Benzaazoua M. The effect of microstructural evolution on the physical properties of paste backfill. In: The 8th international conference on tailings and mine waste, Vail, Forth Collins, Colorado, USA, Balkema; 2001. p. 365–74.
[32] Ait-Mokhtar A, Amiri O, Dumargue P, Sammartino S. A new model to calculate water permeability of cement-based materials from MIP results. Adv Concr Res 2002;13(1):1–7.
[33] Benzaazoua M. Caractérisation physico-chimique et minéralogique de produits miniers sulfures en vue de la réduction de leur toxicité et de leur valorisation. Ph.D. Thesis. INPL, France; 1996.
[34] Ramlochan T, Grabinsky MW, Hooton RD. Microstructural and chemical investigations of cemented paste backfills. In: The 57th canadian geotechnical conference, Quebec City; October 24–27, 2004. p. 293–304.
[35] Ouellet S, Bussière B, Aubertin M, Benzaazoua M. Microstructural evolution of cemented paste backfill: Mercury intrusion porosimetry test results. Cem Concr Res 2007;37(12):1654–65.
[36] Ouellet S, Bussière B, Aubertin M, Benzaazoua M. Characterization of cemented paste backfill pore structure using SEM and IA analysis. Bull Eng Geol Environ 2008;67(2):139–52.
[37] El Aatar O, Belem T, Bussiere B, Benzaazoua M, Yilmaz E. Microstructural properties of column consolidated paste backfill. In: The 60th canadian geotechnical conference, Ottawa, CA; October 21–24, 2007. p. 45–52.
[38] Deschamps T, Benzaazoua M, Bussière B, Aubertin M, Belem T. Microstructural and geo-chemical evolution of paste tailings in surface disposal. Miner Eng 2008;21(4):341–53.
[39] Fall M, Samb SS. Pore structure of cemented tailings materials under natural or accidental thermal loads. Mater Charact 2008;59(5):598–605.
[40] Yilmaz E, Belem T, Bussiere B, Benzaazoua M. Evaluation of strength, microstructure and consolidation properties of cemented paste fill using new laboratory equipment. In: The 3rd international symposium on mines and the environment, Rouyn-Noranda, Quebec, Canada; November 2–5, 2008c.
[41] ASTM Designation D4318-84. Standard test method for liquid limit, plastic limit, and plasticity index of soils. In: Annual book of ASTM standards, vol. 04–08; 1991a. p. 573–83.
[42] McCarthy DF. Essentials of soil mechanics and foundations: basic geotechnics. 7th ed. Pearson-Prentice Hall; 2007.
[43] Yilmaz E. Investigating the consolidation behaviour and hydromechanical and microstructural properties of cemented paste backfills using the versatile CUAPS apparatus. In: Ph.D. Thesis, Université du Québec en Abitibi-Témiscamingue (UQAT), Rouyn-Noranda, Québec, Canada; 2009. <http://bibliotheque.uqat.ca/documents/theses/erolyilmaz.pdf>.
[44] Petrolito J, Anderson RM, Pigdon SP. A review of binder materials used in stabilized backfills. CIM Bull 2005;98(1085):1–7.
[45] Benzaazoua M, Belem T, Yilmaz E. Novel lab tool for paste backfill. Can Min J 2006;127(3):31-31.
[46] Yilmaz E, Belem T, Benzaazoua M, Bussière B. Assessment of the modified CUAPS apparatus to estimate in situ properties of cemented paste backfill. Geotech Testing J 2010;33(5):351–62.
[47] ASTM Designation C39. Standard test method for compressive strength of cylindrical concrete specimens. In: Annual book of ASTM standards, vol. 04–02; 2002. p. 15–23.
[48] ASTM Designation D4404. Standard test method for determination of pore volume and pore volume distribution of soil and rock by mercury intrusion porosimetry. In: Annual book of ASTM standards, vol. 04–08; 2002. p. 582–86.
[49] Washburn EW. The dynamics of capillary flow. Phys Rev 1921;17(3):273–83.
[50] Galle C. Effect of drying on cement-based materials pore structure as identified by mercury intrusion porosimetry: A comparative study between oven, vacuum, and freeze–drying. Cem Concr Res 2001;31(10):1467–77.
[51] Kumar R, Bhattacharjee B. Study on some factors affecting the results in the use of MIP method in concrete research. Cem Concr Res 2003;33(3):417–24.
[52] IUPAC. Manual of symbols and terminology. Appendix 2, part 1: colloid and surface chemistry. J Pure Appl Chem 1972;31:578.
[53] Xu Yongfu. Surface irregularity of soils in molecular domain. Chaos Solitons Fract 2004;21(2):435–44.
[54] ASTM Designation D6556. Standard test method for carbon black-total and external surface area by nitrogen adsorption. In: Annual book of ASTM standards, vol. 04–08; 2009. p. 411–28.
[55] Aligizaki AK. Pore structure of cement-based materials: testing, interpretation and requirement. Modern Concrete Technology Series; vol. 12, New York: Taylor and Francis; 2006.
[56] Diamond S. Mercury porosimetry: an inappropriate method for the measurement of pore size distributions in cement-based materials. Cem Concr Res 2000;30(10):517–1525.
[57] Cook R, Hover K. Mercury porosimetry of hardened cement pastes. Cem Concr Res 1999;29(6):933–43.
[58] Ouellet S, Bussière B, Mbonimpa M, Benzaazoua M, Aubertin M. Reactivity of an underground mine sulphidic cemented paste backfill. Miner Eng 2006;19(5):407–19.
[59] Benzaazoua M, Belem T, Jolette D. Investigation de la stabilité chimique et de son impact sur la qualité des remblais miniers cimentés. In: IRSST Report No R260, Montréal, Québec, Canada; 2000. p. 1–172.
[60] Taylor HFW. Cement chemistry. New York: Academic Press; 1990.
[61] Kendall K, Howard AJ, Birghall JD. The relation between porosity, microstructure and strength, and the approach to advanced cement-based materials. Philos Trans R Soc London 1983;A310(2):139–53.
[62] Hakkinen T. Influence of slag content on the microstructure, permeability and mechanical properties of concrete. Part 1: microstructural studies and basic mechanical properties. Cem Concr Res 1993;23(2):407–21.
[63] Takahashi T, Yamamoto M, Ioku K, Goto S. Relationship between compressive strength and pore structure of hardened cement pastes. Adv Cem Res 1997;9(33):25–30.
[64] Zhang B. Relationship between pore structure and mechanical properties of ordinary concrete under bending fatigue. Cem Concr Res 1998;28(5):699–711.

[65] Kumar R, Bhattacharjee B. Porosity, pore size distribution and in situ strength of concrete. Cem Concr Res 2003;33(1):155–64.
[66] Lee CY, Lee HK, Lee KM. Strength and microstructural characteristics of chemically activated fly ash–cement systems. Cem Concr Res 2003;33(3):425–31.
[67] Li L, Aubertin M. A general relationship between porosity and uniaxial strength of engineering materials. Can J Civ Eng 2003;30(4):644–58.
[68] Vodak F, Trtik K, Kapicková O, Hoskova S, Demo P. The effect of temperature on strength-porosity relationship for concrete. Constr Build Mater 2004;18(7): 529–34.
[69] Matusinović T, Šipušić J, Vrbos N. Porosity–strength relation in calcium aluminate cement pastes. Cem Concr Res 2003;33(11):1801–6.
[70] O'Farrell M, Wild S, Sabir BB. Pore size distribution and compressive strength of waste clay brick mortar. Cement Concr Compos 2001;23(1):81–91.
[71] Fall M, Pokhare M. Coupled effects of sulphate and temperature on the strength development of cemented tailings backfills: Portland cement-paste backfill. Cement Concr Compos 2010;32(10):819–28.